Picosecond optical limiting in reverse saturable absorbers: a theoretical and experimental study

Richard Lepkowicz, Andrey Kobyakov, David J. Hagan, and Eric W. Van Stryland

School of Optics/Center for Research and Education in Optics and Lasers, University of Central Florida, 4000 Central Florida Boulevard, Orlando, Florida 32816-2700

Received February 23, 2001; revised manuscript received June 29, 2001

We theoretically and experimentally study absorption of picosecond laser pulses in materials described by a four-level system that exhibit reverse saturable absorption (RSA). Using an approximate solution to the rate equations, we derive, analyze, and verify, numerically and experimentally, a single dynamical equation for the spatial evolution of the pulse fluence that includes both the rate equations and the propagation equation. This analytical approach considerably simplifies the study of optical limiting with picosecond pulses and helps to predict the behavior of the nonlinear transmittance, the level of output signal clamping, and a possible turnover from RSA to saturable absorption that restricts the performance of optical limiters based on RSA. The results obtained can also be used to characterize RSA materials by the pump–probe technique. © 2002 Optical Society of America

OCIS codes: 190.4180, 140.3360, 190.4710.

1. INTRODUCTION

Materials that exhibit reverse saturable absorption (RSA), i.e., those with an excited-state absorption cross section that is larger than that of the ground state, have drawn a great deal of interest over the past several years.[1–7] One of the most promising applications of these materials is their potential use as passive optical limiters, i.e., as devices designed to protect sensitive optical elements and eyes from laser-induced damage. For an overview of passive optical limiting see, e.g., Refs. 8 and 9. The nonlinear absorption of RSA materials is exploited to decrease the transmittance of a material at high input energy while the material is kept transparent at low input energy as an ideal optical limiter requires. RSA has been observed in many organic materials (for an overview see, e.g., Ref. 1), and efficient optical limiting has been demonstrated in several materials by use of various optical geometries.[10–14]

The key quantities that determine the absorption coefficient of a material are the time-dependent population densities of the ground and excited states, which, in turn, depend on the parameters of the nonlinear medium and the laser pulse characteristics. The population dynamics are described by multilevel rate equations.[1,15–23] For picosecond input pulses, a three-level system (singlet bands only) allows RSA to be modeled but often fails to match data taken at high input fluences. The addition of a higher-lying fourth level[7,18,22] allows for a better match with data for many materials. The four-level model that we use is shown in Fig. 1.

Finding a general analytical solution to the system of rate and propagation equations represents a fairly difficult problem. Thus the solution is usually obtained numerically for a particular set of parameters.[16–19] However, it is still difficult to gain a basic insight into the properties of the nonlinear absorber. For example, to determine the dependence of the sample transmittance on the input fluence with all other parameters fixed, one has to perform a full integration of the rate equations and the propagation equation for each value of the input fluence. To study the effects of any other parameter (e.g., pulse shape, width, lifetimes, absorption cross sections, sample thickness), one has to repeat the entire set of calculations. Even with contemporary computing capabilities, this task is highly time-consuming.

Alternatively, an assumption of so-called fast absorbers[1] (for which the pulse length is much longer than the lifetime of each excited state) allows for an analytical solution of the problem. Mathematically, this means that the differential rate equations reduce to a set of algebraic equations that can easily be solved.[16–18,22] However, this steady-state, or stationary, solution is not always applicable because it assumes long pulses, so a triplet excited state has to be taken into account for many materials.[1,2,6,15–17,19,20,21,23]

Rather than using the steady-state approach,[16–18,22] in the research reported in this paper we performed a dynamical analysis; we show here that the stationary solution to the rate equations gives only a rough estimate for the absorption of short pulses. We show that the behavior of the limiting curve (dependence of the normalized transmittance on input fluence) can be accurately predicted based on the solution of a single ordinary differential equation (ODE). The analytical results will allow us to understand the effect of each individual parameter on the absorptive properties of the material and accurately predict various phenomena, e.g., turnover from RSA to saturable absorption (SA).[16–18,22]

The paper is organized as follows. In Section 2 we introduce rate equations and useful normalizations. In

0740-3224/2002/010094-08$15.00

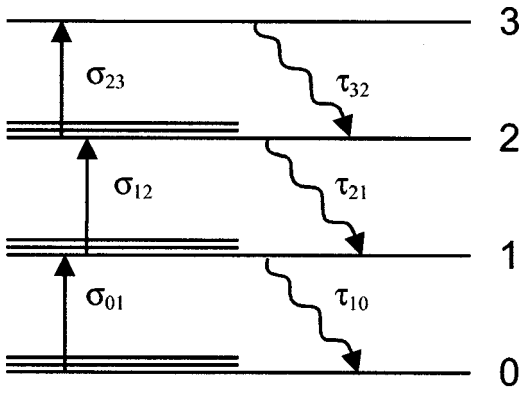

Fig. 1. Schematic diagram of the four-level model of RSA with picosecond pulse illumination; 0 is the ground state and 1–3 are excited singlet states.

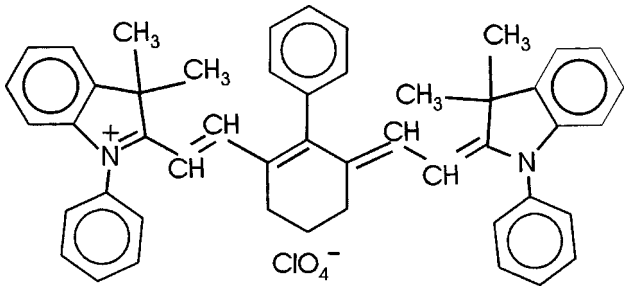

Fig. 2. Chemical structure of dye PD3.

Section 3 we solve the rate equations for a rectangular (flat-topped) input pulse. We then use this solution to study the optical limiting properties of several materials. Particular emphasis is given to the effect of the turnover from RSA to SA and to a comparison of the dynamical solution with predictions of the steady-state analysis. In Section 4 experimental verification of the theoretical analysis is presented for two organic dyes, a carbocyanine dye 1,1′,3,3,3′,3′-hexamethylindotricarbocyanine iodide (HITCI; Refs. 7 and 18) and a polymethine dye (PD3).[3,4] The chemical structure of PD3 is shown in Fig. 2. Section 5 concludes the paper.

2. BASIC EQUATIONS AND NORMALIZATIONS

The model that we use to describe RSA is the singlet state four-level structure depicted in Fig. 1. In as much as we are interested in picosecond excitation we can ignore the triplet states because the intersystem crossing times are typically much longer (>1 ns) than the pulse width.[1] We also neglect the effects that are due to the vibronic sublevels that have subpicosecond relaxation times. In addition, the lifetime τ_{32} is assumed to be much less then the pulse width, which results in negligible population in level 3. As a result, the rate equations can be written as follows[18,22]:

$$\frac{\partial N_0}{\partial t} = -\frac{\sigma_{01} I}{\hbar\omega} N_0 + \frac{N_1}{\tau_{10}},$$

$$\frac{\partial N_1}{\partial t} = \frac{\sigma_{01} I}{\hbar\omega} N_0 - \frac{N_1}{\tau_{10}} - \frac{\sigma_{12} I}{\hbar\omega} N_1 + \frac{N_2}{\tau_{21}},$$

$$\frac{\partial N_2}{\partial t} = \frac{\sigma_{12} I}{\hbar\omega} N_1 - \frac{N_2}{\tau_{21}}, \tag{1}$$

where $N_{0,1,2}$ are the level population densities that are functions of time t and propagation distance z, $N_0 + N_1 + N_2 = N$, $I(z,t)$ is the irradiance of the incident pulse, and $\sigma_{01}, \sigma_{12}, \sigma_{23}$ and $\tau_{10}, \tau_{21}, \tau_{32}$ are the corresponding absorption cross sections and lifetimes (Fig. 1). The population densities determine the spatial pulse evolution by means of the propagation equation[1,16–23]

$$\frac{\partial I}{\partial z} = -I(\sigma_{01} N_0 + \sigma_{12} N_1 + \sigma_{23} N_2). \tag{2}$$

It is easier to deal with Eqs. (1) both numerically and analytically if we recast them into a dimensionless form. First we represent the input irradiance as $I(0,t) = I_0 f(t)$, where I_0 is the peak irradiance and $f(t)$ is a dimensionless function with unit amplitude that reflects the temporal shape of the pulse (e.g., flat-topped, Gaussian, hyperbolic secant). Next we introduce a dimensionless variable that is proportional to the total fluence of the pulse $A = \sigma_{01} I_0 \tau_p / \hbar\omega$ and scale time with pulse width τ_p, i.e., $T = t/\tau_p$. We also introduce absorption cross-section ratios $\alpha = \sigma_{12}/\sigma_{01}$ and $\beta = \sigma_{23}/\sigma_{01}$ and dimensionless ratios $T_{10} = \tau_p/\tau_{10}$ and $T_{21} = \tau_p/\tau_{21}$. Finally, we normalize the level population densities by the total population, $n_j = N_j/N$, where j goes from 0 to 2. Substituting the above definitions into rate equations (1), we arrive at the following set of dimensionless rate equations:

$$\frac{\partial n_0}{\partial T} = -\Phi n_0 + T_{10} n_1,$$

$$\frac{\partial n_1}{\partial T} = \Phi n_0 - (\alpha\Phi + T_{10}) n_1 + T_{21} n_2,$$

$$\frac{\partial n_2}{\partial T} = \alpha\Phi n_1 - T_{21} n_2, \tag{3}$$

where $\Phi = A f(T)$. Further, we define a normalized variable that represents linear absorption $Z = \sigma_{01} N z$,[23] and we express the propagation equation as

$$\frac{\partial \Phi}{\partial Z} = -\Phi(n_0 + \alpha n_1 + \beta n_2). \tag{4}$$

In Section 3 we approximately solve the system of partial differential equations (PDEs) (3) and (4) and verify the results by direct numerical integration of those equations.

3. SOLUTION TO THE RATE EQUATIONS AND NONLINEAR ABSORPTION OF THE RSA MATERIAL

To solve the system of Eqs. (3) and (4) we follow the reasoning of Refs. 1, 19–21 and treat the rate and propagation equations separately. We can solve the former by as-

suming constant irradiances, and we substitute their solution into propagation equation (4). Subsequent integration of both sides of the propagation equation with respect to time will result in the spatial evolution equation for the pulse fluence, $F = \int_{-\infty}^{+\infty} \Phi dT$.[19–21]

It can be expected that, as in the five-level model used for describing the propagation of nanosecond pulses in RSA materials,[1] the functional dependence of the population dynamics on the input fluence does not depend strongly on the pulse shape if the medium is excited by short input pulses.[23] Below, we shall show that the flat-topped pulse approximation $I(t) = I_0$, $0 < t < \tau_p$ (Refs. 1, 20, and 21), provides reasonable accuracy for propagation of realistic laser pulses in many RSA materials, while it greatly simplifies the analysis. In our normalized units, this pulse shape results in $f(T) \equiv 1$, $0 < T < 1$, and Eqs. (3) become a system of ODEs with constant coefficients that are easily solvable.

The standard procedure consists in equating the corresponding determinant of Eqs. (3) to zero to find the eigenvalues. As the order of system (3) equals 3, we obtain a third-order polynomial whose roots can be found explicitly. One of the roots is equal to zero, and the other two are

$$\lambda_{\pm} = (1/2)[-(\alpha + \epsilon + q + 1) \pm \sqrt{D}] < 0, \tag{5}$$

where we have denoted

$$D = \alpha^2 + 2\alpha(q - 1 + \epsilon) + (q - 1 - \epsilon)^2, \tag{6}$$

$\epsilon = T_{10}/A$, and $q = T_{21}/A$.

With eigenvalues known, one can easily find the corresponding eigenvectors and, using the initial conditions for the medium before excitation, $n_0 = 1$, $n_1 = 0$, and $n_2 = 0$, obtain the solution to system (3) as

$$\begin{pmatrix} n_0 \\ n_1 \\ n_2 \end{pmatrix} = C \begin{bmatrix} q & -\dfrac{(\lambda_- + q)\lambda_+}{\sqrt{D}(\lambda_- + 1)} & \dfrac{(\lambda_+ + q)\lambda_-}{\sqrt{D}(\lambda_+ + 1)} \\ \dfrac{q}{\epsilon} & -\dfrac{(\lambda_- + q)\lambda_+}{\sqrt{D}\epsilon} & \dfrac{(\lambda_+ + q)\lambda_-}{\sqrt{D}\epsilon} \\ \dfrac{\alpha}{\epsilon} & -\dfrac{\alpha\lambda_+}{\sqrt{D}\epsilon} & \dfrac{\alpha\lambda_-}{\sqrt{D}\epsilon} \end{bmatrix} \times \begin{bmatrix} 1 \\ \exp(\lambda_- AT) \\ \exp(\lambda_+ AT) \end{bmatrix}, \tag{7}$$

where

$$C = \frac{(\lambda_+ + 1)(\lambda_- + 1)}{\lambda_+\lambda_-(q - 1)}. \tag{8}$$

The solution remains continuous with $T_{21} = A$, i.e., $q = 1$, because both the numerator and the denominator in Eq. (8) approach zero. In the limit $q = 1$, Eq. (7) simplifies to

$$\begin{pmatrix} n_0 \\ n_1 \\ n_2 \end{pmatrix} = \begin{bmatrix} \dfrac{\epsilon}{\alpha + \epsilon + 1} & \dfrac{\epsilon}{(\alpha + \epsilon + 1)(\alpha + \epsilon)} & \dfrac{\alpha}{\alpha + \epsilon} \\ \dfrac{1}{\alpha + \epsilon + 1} & -\dfrac{1}{\alpha + \epsilon + 1} & 0 \\ \dfrac{\alpha}{\alpha + \epsilon + 1} & \dfrac{\alpha}{(\alpha + \epsilon + 1)(\alpha + \epsilon)} & -\dfrac{\alpha}{\alpha + \epsilon} \end{bmatrix} \times \begin{bmatrix} 1 \\ \exp[-(\alpha + \epsilon + 1)AT] \\ \exp(-AT) \end{bmatrix}.$$

To study the spatial evolution of the pulse, we must substitute solution (7) into the propagation equation [Eq. (4)]. The resultant equation is too cumbersome to work with analytically. However, we can significantly simplify the exact solution to rate equations (7) without any substantial reduction in accuracy by examining typical RSA material parameters. Indeed, for a typical RSA material the lifetime of the first excited state, τ_{10}, is of the order of a nanosecond, whereas that of τ_{21} is several picoseconds.[3,7,18] This means that the parameter $\epsilon < 10^{-2}$ is small compared with both q and α ($\alpha > 1$ for RSA materials). Hence we can make a series expansion with respect to ϵ and write Eqs. (5), (6), and (8) as

$$\lambda_+ \approx -1 + \epsilon\frac{1 - q}{\alpha + q - 1},$$

$$\lambda_- \approx -\alpha - q - \epsilon\frac{\alpha}{\alpha + q - 1}, \tag{9}$$

$$\sqrt{D} \approx \alpha + q - 1 + \epsilon\frac{\alpha - q + 1}{\alpha + q - 1}, \tag{10}$$

$$C \approx \frac{\epsilon}{\alpha + q}, \tag{11}$$

respectively. Substituting relations (9)–(11) into Eq. (7) results in the approximate solution to the rate equations. Furthermore, we take advantage of the fact that the solution found for the population densities has two quite different characteristic times, which are proportional to the eigenvalues λ_+ and λ_-. As can be recognized from Eq. (9), $|\lambda_-| \gg |\lambda_+|$, so one can neglect the transient processes that vary as $\sim\exp(\lambda_- AT)$. As a result the approximate solution for the population densities can be expressed in the form

$$n_0(T) \approx \exp(-AT), \tag{12}$$

$$n_1(T) \approx \frac{q}{\alpha + q} + \frac{1 - q}{\alpha + q - 1}\exp(-AT), \tag{13}$$

$$n_2(T) \approx \frac{\alpha}{\alpha + q} - \frac{\alpha}{\alpha + q - 1}\exp(-AT). \tag{14}$$

To check the accuracy of the approximate solutions to the rate equations we compare formulas (12)–(14) with the exact solutions, Eqs. (5)–(8). The results are shown in Fig. 3 for two RSA materials, the carbocyanine dye HITCI (Ref. 7) and the polymethine dye PD3.[3] It can be seen

clearly from Fig. 3 that formulas (12)–(14) accurately describe the population dynamics. The slight initial deviation for n_1 and n_2 is due to the discarded terms that are proportional to $\sim\exp(\lambda_{-}AT)$. It will not have a significant effect on the propagation equation because excited-state populations n_1 and n_2 are small for $T < 0.05$.

To validate the use of a flat-topped pulse we examine the propagation of a pulse through the two RSA materials from Fig. 3 and compare the output fluence as a function of propagation distance for the flat-topped and Gaussian shapes. From Fig. 4 we can conclude that attenuation of total fluence F is nearly the same for both flat-topped and Gaussian pulses. Thus, using a flat-topped shape in solving the rate equations is appropriate and accurately predicts the transmitted fluence of the corresponding short pulses.

Integrating Eq. (4) with formulas (12)–(14), we obtain the propagation equation for the fluence:

$$\frac{dF}{dZ} = \left[\alpha\frac{(\beta-\alpha)F}{(\alpha-1)F+T_{21}} + \alpha - 1\right](1-e^{-F}) - \alpha\left[1+\frac{(\beta-\alpha)F}{\alpha F+T_{21}}\right]F = -\sigma_{\text{eff}}(F)F, \qquad (15)$$

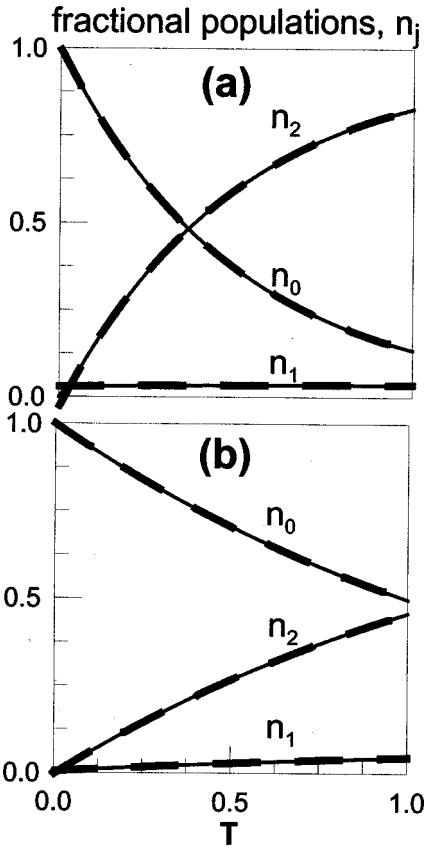

Fig. 3. Population dynamics of two RSA materials excited by a temporal flat-topped pulse with a pulse width of $\tau_p = 25$ ps (FWHM). The results were obtained by use of the exact analytical solution to the rate equations, [Eq. (7); solid curves] and the approximate analytical solution [formulas (12)–(14); dashed curves]. The parameters are (a) for HITCI: $A = 2$, $\alpha = 32$, $\beta = 0.1$, $\tau_{10} = 1.7$ ns, and $\tau_{21} = 10$ ps and (b) for PD3: $A = 0.7$, $\alpha = 200$, $\beta = 2$, $\tau_{10} = 1$ ns, $\tau_{21} = 1.9$ ps. Each material has a linear transmittance of 0.905 ($Z = 0.1$).

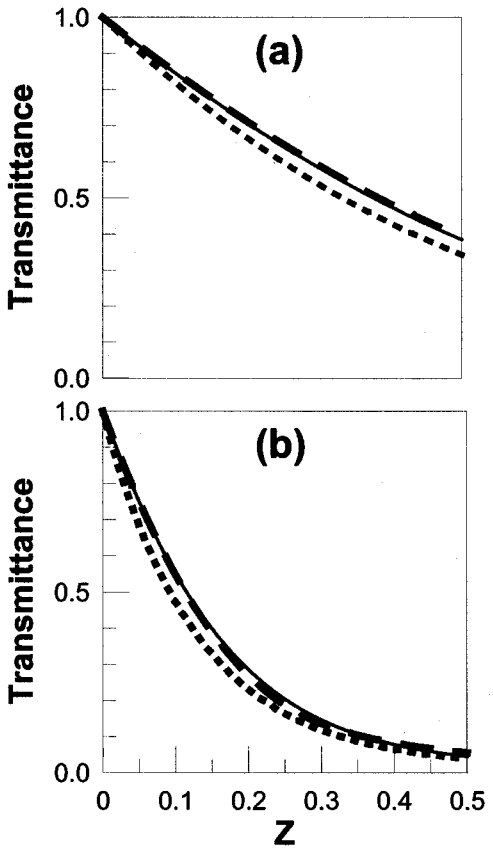

Fig. 4. Transmittance ($F_{\text{out}}/F_{\text{in}}$) as a function of normalized propagation distance $Z = \sigma_{01}Nz$ for the dyes in Fig. 3: (a) HITCI, (b) PD3. Dotted and dashed curves, the numerical solutions to Eqs. (3) and (4) for a Gaussian (FWHM, $\tau_p = 23.5$ ps) and a flat-topped pulse shape, respectively. Solid curves, numerical solution to ODE (15).

where $F = \int_{-\infty}^{+\infty}\Phi dT$ and $\sigma_{\text{eff}}(F) = (1/F)\int_0^F(n_0 + \alpha n_1 + \beta n_2)dF$ is the effective fluence cross section.[19,23] Note that this single differential equation now includes both the set of rate equations and the propagation equation. Equation (15) cannot be solved analytically, but its numerical solution represents a much easier task than solution of the full system [Eqs. (3) and (4)] for every value of input fluence. The results of numerical integration of Eq. (15) are shown in Fig. 4 by the solid curves.

We also computed limiting curves (transmittance versus input fluence) for HITCI and PD3. We compared the numerical solution to Eq. (15) with the full set of rate and propagation equations (3) and (4) for a flat-topped and a Gaussian input pulse. The solution to Eq. (15) almost coincides with the numerical solution to the original system with the flat-topped input, and it is also close to the numerical solution for a corresponding (equal total fluence and peak irradiance) Gaussian pulse (Fig. 5).

The important feature to notice in the limiting curves is the effect of turnover from RSA to SA.[18,22] As can be seen from Fig. 5, the turnover predicted by Eq. (15) occurs at slightly lower fluences than that given by the numerical solution to the original system of Eqs. (3) and (4). Thus, our solution predicts a lower limit of the input fluence when this turnover occurs for a more realistic pulse shape. An approximate condition for the turnover point

(F_{to}) in terms of the material parameters can be obtained as a solution to $d\sigma_{eff}(F)/dF = 0$.[22] This criterion provides good accuracy only for low linear losses (less than 10%) and can be expressed in terms of the transcendental equation

$$\begin{aligned}&\alpha(\beta - \alpha)T_{21}F^2(\alpha F - F + T_{21})^2 \\ &\quad + T_{21}F(\alpha F + T_{21})^2(1 - e^{-F})(\alpha^2 - \alpha\beta) \\ &\quad + [(F + 1)e^{-F} - 1](\alpha F - F + T_{21})(\alpha F + T_{21})^2 \\ &\quad \times [(2\alpha - \alpha\beta - 1)F - (\alpha - 1)T_{21}] = 0, \end{aligned} \tag{16}$$

whose numerical solution F_{to} gives the turnover fluence.

To complete our analysis, we compare our results with those obtained previously[18,22] that exploit the steady-state solution to rate equations (3). Using the normalization procedure from Section 2, we arrive at the following propagation equation, obtained with the stationary population densities[22]:

$$\frac{d\tilde{A}}{dZ} = \frac{-\tilde{A}(V + \alpha\tilde{A} + \beta\alpha\tilde{A}^2)}{V + \tilde{A} + \alpha\tilde{A}^2}, \tag{17}$$

where $\tilde{A} = \sigma_{01}I_0\tau_{21}/\hbar\omega = A/T_{21}$ and $V = \tau_{21}/\tau_{10}$. In Fig. 6 we have plotted the limiting curve for HITCI calculated from the dynamical propagation [Eq. (15)] and from the steady state [Eq. (17)]. It is clear that the latter predicts much stronger limiting and an even earlier turnover from RSA to SA than that predicted by the dynamical model [Eq. (15)]. As can be inferred from Fig. 6, the shape of the limiting curve predicted by the steady-state model differs strongly from the results of the dynamical analysis. It can be expected that the steady-state model will predict a much lower transmittance at higher input fluences, but what is surprising is that the value of the fluence at the minimum in transmittance (the turnover point) is in most cases an order of magnitude less than that given by the dynamical model.

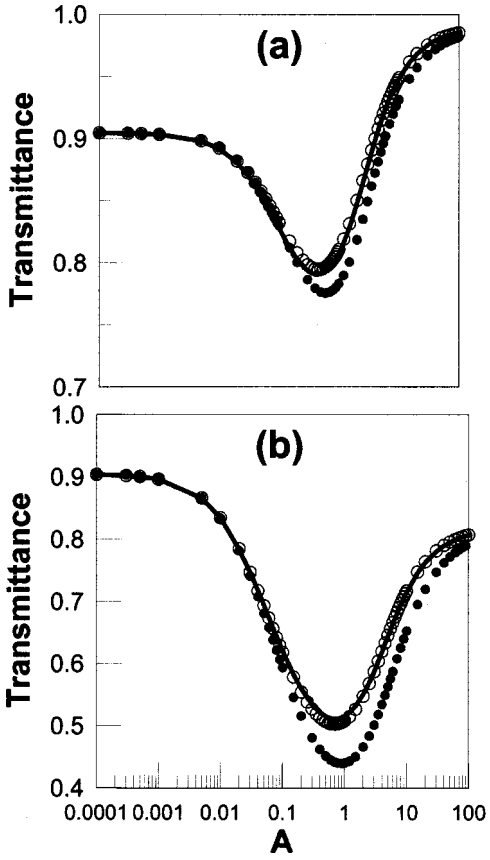

Fig. 5. Transmittance (F_{out}/F_{in}) as a function of normalized input fluence for the dyes in Fig. 3: (a) HITCI, (b) PD3. Solid curves, limiting curves calculated by use of the numerical solution to ODE (15). Open and solid circles, limiting curves calculated from the full system of PDEs (3) and (4) for flat-topped and Gaussian pulses, respectively.

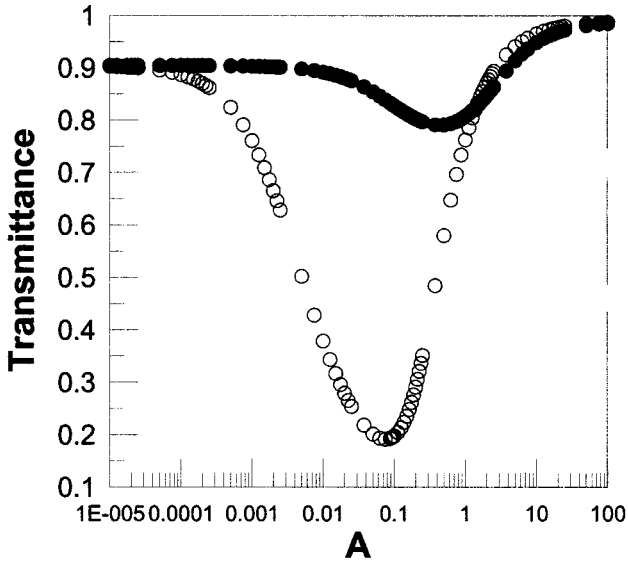

Fig. 6. Limiting curves calculated for HITCI from the numerical solution to Eq. (15) derived from the dynamical solution to the rate equations (filled circles) and the numerical solution to Eq. (17) derived from the steady-state solution to the rate equations (open circles). Pulse width, (FWHM) 25 ps.

4. EXPERIMENT AND DISCUSSION

To confirm the theoretical predictions developed in Section 4 we performed optical limiting experiments with an active–passive mode-locked Nd:YAG laser that operates at a 10-Hz repetition rate. The fundamental wave of the Nd:YAG laser was doubled to 532 nm, and a single 25 ps (FWHM) pulse was switched out from the 56-ns-long pulse train. The beam waist was measured by the thin-sample Z-scan technique[24] and checked with a CCD camera to be approximately 20 μm (half-width at $1/e^2$ max). Each sample was placed at the focal plane determined from an open-aperture Z-scan measurement of the sample. The input energy was varied from 1 nJ to 10 μJ by a stepper motor attached to a half-wave plate in front of a fixed polarizer.

In the previous sections of this paper we reported using the materials HITCI and PD3 to compare the theoretical and numerical results. We have experimentally studied these two materials along with the phthalocynaine dye chloroaluminum phthalocynaine (CAP).[6] With the exception of HITCI,[7] we could not find any references to measured values of the second excited-state cross section σ_{23}. Therefore we performed the experiment on HITCI

to compare with previous results[7,18] and on PD3 and CAP to determine σ_{23} from fitting the experimentally measured limiting curve. Also, the experimentally determined value of the fluence at the turnover point can be compared with that predicted by the dynamical and steady-state solutions. It will be seen that HITCI and PD3 fit the model exploited in this paper quite well but that CAP does not.

The results of the optical limiting experiments for HITCI and PD3 are shown in Figs. 7(a) and 7(b), respectively. The experimental results are plotted along with the limiting curves produced by the numerical solution of Eqs. (3) and (4) for a Gaussian pulse and the solution to the ODE.[15] The best-fit parameters for HITCI ($\sigma_{01} = 2.5 \times 10^{-17}\,\mathrm{cm}^2$, $\sigma_{12} = 87.5 \times 10^{-17}\,\mathrm{cm}^2$, $\sigma_{23} = 1.5 \times 10^{-17}\,\mathrm{cm}^2$, $\tau_{10} = 1.7 \times 10^{-9}$, $\tau_{21} = 2.2 \times 10^{-12}$, $Z = 0.091$) and for PD3 ($\sigma_{01} = 1.03 \times 10^{-18}\,\mathrm{cm}^2$, $\sigma_{12} = 2.2 \times 10^{-16}\,\mathrm{cm}^2$, $\sigma_{23} = 5.2 \times 10^{-20}\,\mathrm{cm}^2$, $\tau_{10} = 1.0 \times 10^{-9}$, $\tau_{21} = 6.0 \times 10^{-12}$, $Z = 0.089$) are in good agreement with previously reported results for HITCI (Ref. 18) and for (PD3)[3,4] We then determined the fluence at the turnover point from Fig. 7 for the experiment and the two fitting curves. We also calculated the fluence at the turnover point, using transcendental equation (16) and the numerical solution to the steady-state propagation, Eq. (17). The values for the fluence at the turnover point for both HITCI and PD3 obtained with all the methods described above are listed in Table 1. As can be seen from Fig. 7 and Table 1, all the predicted values for the fluence at the turnover point are lower than those of the experimental results. It has been shown for HITCI (Refs. 7 and 18) and for PD3 (Refs. 3 and 4) that to explain nonlinear absorption in these materials one needs to use a more detailed model structure. For HITCI, Hughes and Wherrett[18] and Swatton *et al.*[7] have shown that their experimental data could be fitted accurately if they accounted for a finite intraband vibrational lifetime. As for PD3, Lim *et al.*[3] and Przhonska *et al.*[4] showed that an all-singlet state five-level model, which includes reorientational processes in the first excited state, would accurately fit their experimental data. Even neglecting these details, our dynamical solution approximately predicts the fluence at the turnover point to the same order of magnitude. For the material CAP our model could not fit the data (Fig. 8) and therefore does not make accurate predictions of the fluence at the turnover point. Wei *et al.*[6] had to invoke both two-photon absorption and excited-state absorption to fit their data accurately. So in this case the two-photon absorption is large enough that it cannot be neglected.

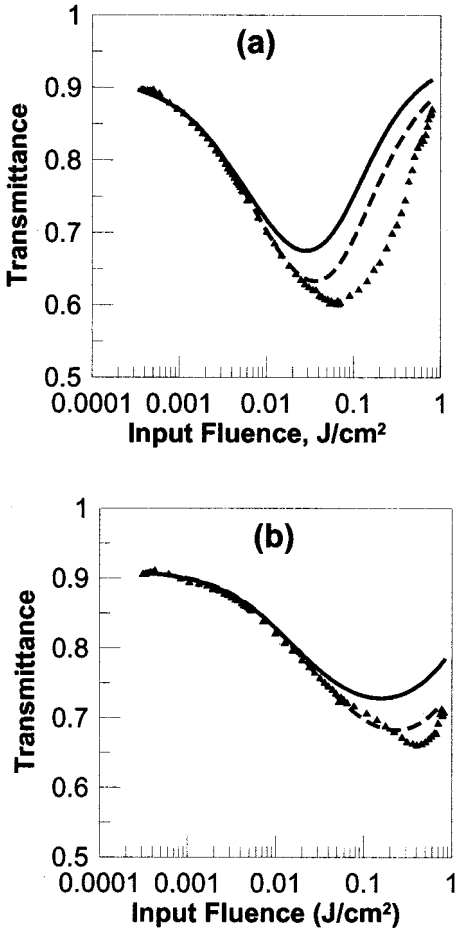

Fig. 7. Experimentally measured limiting curve (triangles) for (a) HITCI and (b) PD3 with the best-fit material parameters used in the numerical solution to Eq. (15) (solid curves) and the full system of PDEs (3) and (4) for a Gaussian pulse (dashed curves).

Below, we briefly explain how the material parameters effect the behavior of the limiting curve. First, we consider the normalized time parameters T_{21} and T_{10}. As T_{21} becomes larger (longer pulses or shorter lifetime of the second excited state) the limiting curve becomes deeper and the turnover from RSA to SA shifts to higher fluences. However, a change in T_{10} of as much as an order of magnitude barely affects the nonlinear absorption of the material. As for the excited-state cross-section parameters α and β, a larger α (larger first-excited-state cross section or smaller ground-state cross section) produces a deeper limiting curve, but the turnover from RSA to SA does not shift to higher fluences, as was seen with an increase in T_{21}. Parameter β is the most sensitive material parameter for determining when the turnover from RSA to SA will occur. As β increases, the limiting curve becomes slightly deeper and the turnover point

Table 1. Turnover Fluence (mJ/cm^2) Determined from Experimental and Numerical Results

	Method				
Material	Eq. (17)	Eq. (16)	Eq. (15)	Eqs. (3), (4), Gaussian Input	Experiment
HITCI	3	13	27	36	84
PD3	55	76	155	232	414

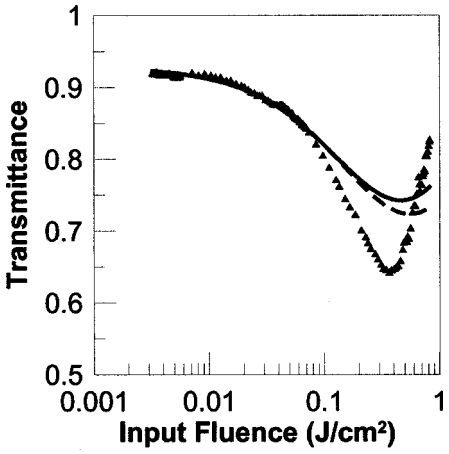

Fig. 8. Experimentally measured limiting curve (triangles) for CAP with best-fit material parameters used in the numerical solution to Eq. (15) (solid curves) and the full system of PDEs (3) and (4) for a Gaussian pulse (dashed curve).

shifts to higher input fluences. It is important to note that all these tendencies rely on the assumption of sufficient linear absorption to populate the first excited level.

Our theoretical results can also be used to analyze the output fluence at high input fluence levels ($F \gg 1$). In this case, an exponential term in Eq. (15) can be dropped and the asymptotic behavior of the output fluence can be obtained from the condition

$$u(F_{\text{out}}) \approx u(F_{\text{in}})\exp[-\alpha(\beta + T_{21})Z], \tag{18}$$

where

$$u(F) = (F - 1)^{T_{21}+\alpha}\left(F + \frac{T_{21}}{\beta}\right)^{T_{21}(\alpha-\beta)/\beta}. \tag{19}$$

For instance, the output becomes clamped at the maximum allowable energy, e.g., 1 μJ can be achieved for 25-ps pulses by use of the polymethine dye PD3[3,4] with 80% linear transmittance and $\alpha = 50$ if $\beta > \beta_{\text{cr}} \approx 28$.

An important conclusion to make is that for high input energies with sufficient linear absorption the key parameter that influences optical limiting is the ratio of the second excited-state absorption cross section to the ground-state absorption cross section. In the above example the output energy is merely changed, with the increase in α from 50 to 200. Therefore, from the viewpoint of efficient picosecond optical limiting, there is no advantage in having a large first-excited-state absorption cross section with a small second-excited-state absorption cross section because the latter will act as a bottleneck to the optical limiting process. Recently synthesized polymethine dyes that have a large first-excited state absorption cross section are quite poor optical limiters in the picosecond regime because of a low value of β. This consideration needs to be taken into account when one is synthesizing new materials for optical limiting. The qualitative basis for practical estimates can be gained from formula (18).

5. CONCLUSIONS

In the picosecond regime the steady-state solution to the rate equations does not always provide a reasonably accurate description of the nonlinear absorption in RSA materials, whereas numerical treatment of the full system of PDEs remains time-consuming. We have developed an approach that accounts for the dynamical behavior of the population densities and optical propagation but requires only the numerical solution of a single ODE. We have shown that the specific pulse shape has little effect on the nonlinear absorption of the pulse, so a flat-topped pulse shape can be used that greatly simplifies and expedites modeling of beam propagation through RSA materials with picosecond pulses. We have obtained an approximate criterion for the turnover from RSA to SA to rapidly calculate the turnover point from the photophysical properties of the material. The dynamical equation for fluence allows us to determine the critical values of material parameters to achieve the output energy clamping at the desired level. This approach can be straightforwardly extended to the case of arbitrary initial conditions to study the absorption properties of the material by double pump–probe measurements.[25,26] Additionally, we can use the results of picosecond optical limiting experiments to determine material parameters that in turn can then be used to predict the outcome of nanosecond optical limiting.

ACKNOWLEDGMENTS

The authors gratefully acknowledge the support of the National Science Foundation (grant 9970078), the U.S. Office of Naval Research (grant N00014-97-1-0936), and the Naval Air Warfare Center Joint Service Agile Program (contract N00421-98-C-1327). The authors thank Olga V. Przhonska for providing the PD3 dye.

R. Lepkowicz's e-mail address is rlepkowi @mail.ucf.edu.

REFERENCES

1. J. W. Perry, "Organic and metal-containing reverse saturable absorbers for optical limiters," in *Nonlinear Optics of Organic Molecules and Polymers*, H. S. Nalwa and S. Miyata, eds. (CRC Press, Boca Raton, Fla., 1997), pp. 813–840.
2. K. R. Welford, S. N. R. Swatton, S. Hughes, S. J. Till, G. Spruce, R. C. Hollins, and B. S. Wherrett, "Nonlinear absorption in organic dyes," Mater. Res. Soc. Symp. Proc. **374**, 239–256 (1995).
3. J. H. Lim, O. V. Przhonska, S. Khodja, S. Yang, T. S. Ross, D. J. Hagan, E. W. Van Stryland, M. V. Bondar, and Y. L. Slominsky, "Polymethine and squarylium molecules with large excited-state absorption," Chem. Phys. **245**, 79–97 (1999).
4. O. V. Przhonska, J. H. Lim, D. J. Hagan, E. W. Van Stryland, M. V. Bondar, and Y. L. Slominsky, "Nonlinear light absorption of polymethine dyes in liquid and solid media," J. Opt. Soc. Am. B **15**, 802–809 (1998).
5. K. Dou, X. Sun, X. Wang, R. Parkhill, Y. Guo, and E. T. Knobbe, "Optical limiting and nonlinear absorption of excited states in metalloporphyrin-doped sol gels," IEEE J. Quantum Electron. **35**, 1004–1014 (1999).
6. T. H. Wei, T. H. Huang, and T. C. Wen, "Mechanism of reverse saturable absorption in chloro-aluminium phthalocyanine solution studied with Z-scan," Chem. Phys. Lett. **314**, 403–410 (1999).
7. S. N. R. Swatton, K. R. Welford, S. J. Till, and J. R. Sambles, "Nonlinear absorption of a carbocyanine dye

1,1′,3,3,3′,3′-hexamethylindotricarbocyanine iodide using a Z-scan technique," Appl. Phys. Lett. **66**, 1868–1870 (1995).
8. L. W. Tutt and T. F. Boggess, "A review of optical limiting mechanisms and devices using organics, fullerenes, semiconductors and other materials," Prog. Quantum Electron. **17**, 299–338 (1993).
9. E. W. Van Stryland, D. J. Hagan, T. Xia, and A. A. Said, "Application of nonlinear optics to passive optical limiting" in *Nonlinear Optics of Organic Molecules and Polymers*, H. S. Nalwa and S. Miyata, eds., (CRC Press, Boca Raton, Fla., 1997), pp. 840–860.
10. J. W. Perry, K. Mansour, Y. S. Lee, X. L. Wu, P. V. Bedworth, C. T. Chen, D. Ng, S. R. Marder, P. Miles, T. Wada, M. Tian, and H. Sasabe, "Organic optical limiter with a strong nonlinear response," Science **273**, 1533–1536 (1996).
11. J. S. Shirk, R. G. S. Pong, S. R. Flom, F. J. Bartoli, M. E. Boyle, and A. W. Snow, "Lead phthalocyanine reverse saturable absorption optical limiters," Pure Appl. Opt. **5**, 701–707 (1996).
12. F. E. Hernández, S. Yang, E. W. Van Stryland, and D. J. Hagan, "High-dynamic-range cascaded-focus optical limiter," Opt. Lett. **25**, 1180–1182 (2000).
13. J. Oberle, L. Bramerie, G. Jonusauskas, and C. Rulliere, "Optical-limiting properties of a push-pull diphenylbutadiene," Opt. Commun. **169**, 325–332 (1999).
14. D. J. Hagan, T. Xia, A. A. Said, T. H. Wei, and E. W. Van Stryland, "High dynamic range passive optical limiters," Int. J. Nonlinear Opt. Phys. **2**, 483–501 (1993).
15. M. Hercher, "An analysis of saturable absorbers," Appl. Opt. **6**, 947–954 (1967).
16. C. Li, L. Zhang, M. Yang, H. Wang, and Y. Wang, "Dynamic and steady- state behaviors of reverse saturable absorption in metallophthalocyanine," Phys. Rev. A **49**, 1149–1157 (1994).
17. C. Li, J. Si, M. Yang, R. Wang, and L. Zhang, "Excited-state nonlinear absorption in multi-energy-level molecular systems," Phys. Rev. A **51**, 569–575 (1995).
18. S. Hughes and B. Wherrett, "Multilevel rate equation analysis to explain the recent observations of limitations to optical limiting dyes," Phys. Rev. A **54**, 3546–3552 (1996).
19. T. Xia, D. J. Hagan, A. Dogariu, A. Said, and E. W. Van Stryland, "Optimization of optical limiting devices based on excited state absorption," Appl. Opt. **36**, 4110–4122 (1997).
20. P. Miles, "Bottleneck optical pulse limiters revisited," Appl. Opt. **38**, 566–570 (1999).
21. P. Miles, "Bottleneck optical limiters: the optimal use of excited-state absorbers," Appl. Opt. **33**, 6965–6979 (1994).
22. X. Deng, X. Zhang, Y. Wang, Y. Song, S. Liu, and C. Li, "Intensity threshold in the conversion from reverse saturable absorption to saturable absorption and its application in optical limiting," Opt. Commun. **168**, 207–212 (1999).
23. A. Kobyakov, D. J. Hagan, and E. W. Van Stryland, "Analytical approach to dynamics of reverse saturable absorbers," J. Opt. Soc. Am. B **17**, 1884–1893 (2000).
24. M. Sheik-Bahae, A. A. Said, T. H. Wei, D. J. Hagan, and E. W. Van Stryland, "Sensitive measurement of optical nonlinearities using a single beam," IEEE J. Quantum Electron. **26**, 760–769 (1990).
25. S. N. R. Swatton, K. R. Welford, R. C. Hollins, and J. R. Sambles, "A time resolved double pump-probe experimental technique to characterize excited-state parameters of organic dyes," Appl. Phys. Lett. **71**, 10–12 (1997).
26. J. Schell, D. Ohlmann, D. Brinkmann, R. Levy, M. Joucla, J. L. Rehspringer, and B. Honerlage, "Reverse saturable absorption in C_{60}-doped porous glasses studied by single- and double-pulse pump-probe experiments," J. Chem. Phys. **111**, 5929–5937 (1999).